CONTROLLING STRAIN ENERGY DENSITY IN 3D CELLULAR COLLAGEN CONSTRUCTS DURING COMPLEX LOADS

by

Katherine Hollar

A thesis

submitted in partial fulfillment

of the requirements for the degree of

Master of Science in Mechanical Engineering

Boise State University

December 2019

BOISE STATE UNIVERSITY GRADUATE COLLEGE

DEFENSE COMMITTEE AND FINAL READING APPROVALS

of the thesis submitted by

Katherine Hollar

Thesis Title: Controlling Strain Energy Density in 3D Cellular Collagen Constructs During Complex Loads

Date of Final Oral Examination: 23 August 2019

The following individuals read and discussed the thesis submitted by student Katherine Hollar, and they evaluated her presentation and response to questions during the final oral examination. They found that the student passed the final oral examination.

Trevor Lujan, Ph.D.	Chair, Supervisory Committee
Gunes Uzer, Ph.D.	Member, Supervisory Committee
Clare Fitzpatrick, Ph.D.	Member, Supervisory Committee
Richard Beard, Ph.D.	Member, Supervisory Committee

The final reading approval of the thesis was granted by Trevor Lujan, Ph.D., Chair of the Supervisory Committee. The thesis was approved by the Graduate College.

DEDICATION

This thesis is dedicated to my loving family, who have instilled in me the virtues of diligence, ambition, and curiosity. Στον Ανδρέα Σάββα, ευχαριστώ για την αγάπη, την υπομονή, και τα σοφά λόγια σου.

ACKNOWLEDGEMENTS

This research was supported by the Institutional Development Awards (IDeA) from the National Institute of General Medical Sciences of the National Institutes of Health under Grants No. P20GM103408 and P20GM109095. We also acknowledge support from The Biomolecular Research Center at Boise State with funding from the National Science Foundation Grants No. 0619793 and 0923535, the MJ Murdock Charitable Trust, and the Idaho State Board of Education. Furthermore, this research project was based on work supported by the National Science Foundation Graduate Research Fellowship under Grant No. 1545659.

I would like to thank Dr. Trevor Lujan for his years of guidance and encouragement. Additionally, I would like to express gratitude to Dr. Gunes Uzer for the access to a cell culture facility and supplies as well as Stephanie Tuft for all the cell culture training. I am also very appreciative for all my lab colleagues, who have provided a collaborative and supportive work environment.

ABSTRACT

Mechanical stimulation applied to damaged soft tissues, such as ligament, can promote tissue remodeling to accelerate healing. To help identify treatments that encourage ligament healing, bioreactors have been designed to subject 3D cellularized constructs to various loading conditions in order to determine the mechanical mechanisms that trigger cell-mediated repair. An innovative approach is to use a bioreactor to apply controlled states of biaxial stress to study the effects of strain energy density and distortion energy on cell activity. Tissue distortion has been linked to changes in the structure and function of ligament, yet the specific impact of distortion energy on cell response has not been quantified. This is due to challenges in establishing a method to apply targeted levels of strain energy density to cellularized constructs.

The goal of this study was to develop a novel methodology of subjecting 3D cellularized constructs to differing magnitudes of distortion energy while maintaining a targeted strain energy density. To vary the levels of distortion energy, the 3D cellular constructs were subjected to simple and complex loading conditions using a biaxial bioreactor. The bioreactor was able to accurately apply a targeted strain energy density of 300 J/m^3 to the constructs during the various loading conditions with an average error of 12.7%. The complex loading conditions generated over 2-fold greater distortion energy than the simple loading conditions and was 22% greater when fibroblast cells were present. For the first time, this study has developed an experimental methodology to

control the total strain energy density in a localized region of 3D cellular constructs as well as quantify the distortion energy in these constructs.

TABLE OF CONTENTS

LIST OF TABLES

LIST OF FIGURES

LIST OF ABBREVIATIONS

2D	Two-dimensional
3D	Three-dimensional
ε	Strain
σ	Stress
W	Strain energy density

CHAPTER ONE: INTRODUCTION

Motivation

Ligaments are fibrous bands of connective tissue that attach bones to other bones to provide joint stability and prevent movement that may damage joint articular cartilage. Through overuse and abnormal joint loading, ligaments are highly susceptible to tears. These injuries make up over 15 million hospital visits a year, which corresponds to an annual cost of 3 billion dollars [1–4]. Furthermore, ligament tissue is slow to heal and recover to their original strength due to fibrous tissue being poorly vascularized [5,6]. In fact, approximately ⅓ of people that have suffered a ligament injury will continue to experience symptoms, such as pain and restricted joint motion, for 3 or more years [7]. In the long-term, the decreased strength of the repaired tissue can lead to repeated injuries and gait pattern alterations [8], which can result in the early onset of osteoarthritis. The main cause of these functional impairments is the poor structural condition of the healed tissue [9]. In healing tissue, the collagen fibers are only slightly aligned and, thus, are weaker than native ligament, which has highly aligned fibers [10]. However, previous studies have shown that mechanical stimulus to ligament may increase tissue stiffness and strength by promoting fibroblast activity [11,12], which are cells responsible for the production and repair of ligament collagen networks. Therefore, numerous studies have investigated the optimal loading conditions for the production and organization of collagen [13–15]. A typical experimental model for these studies has been fibroblast-seeded three-dimensional (3D) constructs tested within a tissue engineering bioreactor,

which is a mechanical test system that applies dynamic loads in a controlled biological environment. Yet, the specific types of matrix stress and deformation to apply in order to promote fibroblast activity remains unknown. Thus, prior research has investigated how applied loads impact cell response, where uniaxial tension is the most common loading condition studied [15–17]. However, these studies have been challenged with successfully identifying a singular theory on the relationship between cell behavior and mechanical stimulation. A novel and potentially advantageous strategy is to investigate how cells respond to strain energy density, which is the stored energy due to deformation. Furthermore, strain energy density can be decoupled into deviatoric (distortion) and dilational (hydrostatic) components. Deviatoric or distortion energy relates to the change in material shape, while dilational or hydrostatic energy relates to the material volume change. Experimentally measuring distortion energy may provide information on cell behavior in response to different types of applied loads, including tension, compression, and complex loads. This method will also allow for the testing of new mechanobiology theories based on strain energy density, which may unify existing theories that currently only account for single directional loads (i.e. only tension, only compression). Presently, research has been challenged with accurately establishing a method to experimentally measure distortion or dilational energy for soft tissues or tissue constructs.

Research Goal

The purpose of this research is to validate a methodology of subjecting 3D fibroblast-seeded constructs to differing magnitudes of distortion energy while maintaining a targeted strain energy density using a biaxial bioreactor. Different loading conditions will be applied by the bioreactor, such as tension, compression, and combined loads, which

vary the amount of distortion energy the constructs experience. Furthermore, non-cellular as well as cellular constructs will be tested to determine how distortion changes with the presence of cells.

Clinical Relevance

This study has the potential to identify the optimal loading conditions for tissue-engineered constructs, which are commonly used to replace damaged soft tissues. Furthermore, this research can guide the development of effective manual therapy techniques used by physical therapists to prevent and treat chronic joint disorders.

CHAPTER TWO: BACKGROUND

2.1 Ligament

2.1.1 Structure, function, and healing

Ligaments are fibrous connective tissue that attach bones to other bones within a joint (**Fig. 1)**. Structurally, ligaments can be broken down into three main components: ground substance, fibers, and cells [18]. The ground substance is an amorphous gel-like material that is composed of water, proteins, and carbohydrate molecules. Furthermore, the ground substance allows for communication and transportation of nutrients between tissues. Ligament fibers are primarily made up of collagen and elastin, which provide great tensile strength and resistance to stretching. Lastly, fibroblast cells play a crucial role in the deposition and remodeling of ground substance and fibers. Therefore, fibroblasts become active during the ligament healing process.

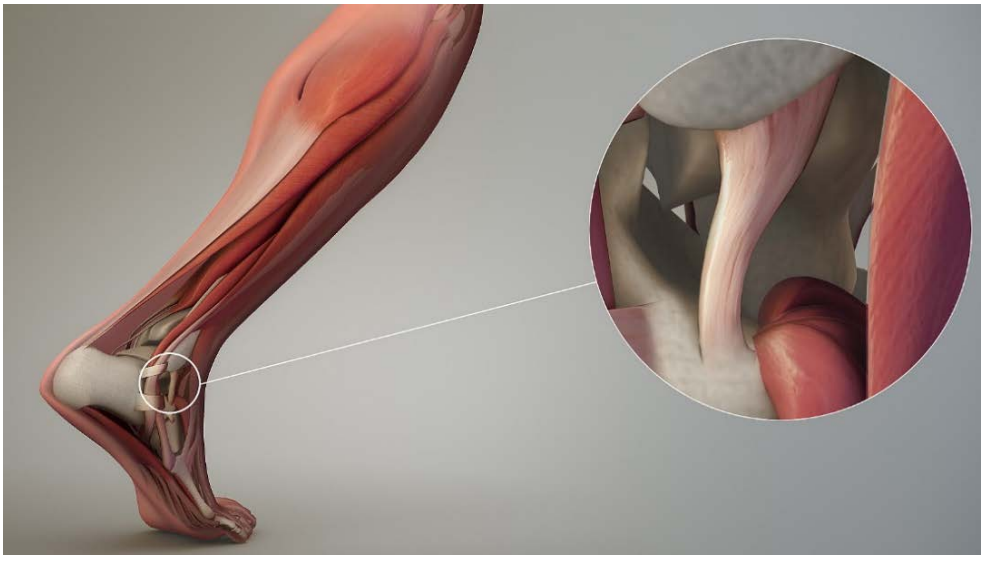

Figure 1 Ligaments in the ankle joint [71]**.**

Functionally, ligaments provide joint stability and prevent movement that can cause damage to the articular cartilage within a joint. Ligament tissue mainly supports mechanical loads in tension, but have been reported to experience compression and shear in ligaments that are concentrically loaded, such as periodontal ligaments [19]. Because ligaments in the knee are frequently injured [20], the physiological strains applied to ligaments have been studied. Knee ligaments, such as the anterior cruciate ligament, can withstand tensile strains up to 6% and forces up to 5% of body weight [21]. However, when a ligament becomes injured, the tissue can no longer support the same magnitude of mechanical loads that healthy ligament allows. Therefore, current research has focused on the process of ligament healing to understand the basic physiological mechanisms of remodeling and repair with the purpose of being able to restore the mechanical integrity of injured ligament [22].

Ligaments heal through a distinct series of cellular events that occur through three successive stages: the acute inflammatory stage, the regenerative stage, and the tissue remodeling stage [18,23]. During the acute inflammatory stage, a blood clot will begin to form at the wound within minutes of the injury to mitigate bleeding. Several growth factors are also released, which increases vascularity at the wound, promote cells to produce collagen and cartilage, and stimulate immune responsive cells to remove debris in the injured tissue. The regenerative stage is then characterized by the wound being rebuilt with disorganized scar tissue. The formation of this scar tissue or granulation tissue is initiated by fibroblasts, which migrate to the wound, proliferate, and deposit a collagen-rich matrix in attempt to close the wound. Once the wound is closed, the regenerative stage begins to transition into the remodeling stage and can last for several

months to as long as a year after the injury. At this stage, the injured tissue begins to resemble normal ligament, but continues to be structurally and functionally different. Some of these differences include poor collagen alignment, high cell and matrix turnover, and smaller collagen fibrils in the injured ligament [23].

2.1.2 Fibroblast-mediated repair due to mechanical stimulus

Fibroblasts are known as mechanosensitive cells, since they can respond to mechanical stimuli or environmental 'cues' by regulating their biochemical activity through a process termed mechanotransduction. Mechanical stimulus to cells, such as fibroblasts, have shown to increase cell proliferation and collagen production [14], which are crucial processes that occur naturally during the regenerative stage of ligament healing (**Table 1**). Thus, the application of mechanical loads, which causes deformation, to fibroblasts can encourage ligament healing. Applying mechanical loads, such as cyclic stretch, triggers specific growth factors to be released from fibroblasts, which then promotes cell proliferation, differentiation and matrix formation to aid in the ligament healing process [24–26]. Therefore, the application of mechanical loads or cell deformation triggers a cascade of cellular responses that accelerate tissue healing. This knowledge of applying mechanical stimulation with the purpose of deforming ligament has been the basis for manual therapy techniques, which use a blunt instrument to dynamically apply compressive forces to damaged tissue to promote fibroblast activity. However, despite manual based therapy being used by 36 million U.S. adults each year, the basic mechanical mechanisms that initiate cellular activity remain unknown. In fact, there is no agreement on the optimal mechanical stimulus or loading strategies (**Table 1**). Previous research has shown that cells will positively respond to being stimulated in

tension, where an increase in cell proliferation and collagen production have been reported [15,16]. Yet, cells stimulated in compression have shown opposite results, where collagen production increases at the expense of cell proliferation [13,27]. Therefore, a consensus must be reached on the loading regimes that best promote cell response in order to advance soft tissue therapy techniques.

Table 1 Impact of mechanical stimulation on cell response.

Study	Cell Source	Scaffold/Explant	Loading Condition	Magnitude	Freq (Hz)	Loading (days)	Loading (hr/day)	Culture composition[a]
Martinez et al., 2011	Murine fibroblasts	Bacterial cellulose (unmodified and micro-channeled)	Compression	5% strain	0.1	14	5	cell proliferation - collagen production +
Torzilli et al, 1996	Canine	Canine articular cartilage explants	Unconfined compression	0.5 to 24 MPa (static and dynamic)	1	Not given	2-24	metabolic response -
Juncosa-Melvin et al, 2007	Rabbit mesenchymal stem cells	Collagen type I sponges	Tension	2.4% strain	Not given	14	8	collagen type I and II +
Webb et al, 2006	Human tracheal fibroblasts	Elastomeric polyurethane	Tension	10% strain (static and cyclic)	0.25	7	8	cell proliferation +

[a] Decrease and increase denoted as – and + compared to static control scaffolds/explants, respectively

2.1.3 Fibroblast-seeded scaffolds

To investigate the optimal loading conditions, fibroblasts have been mechanically stimulated as two-dimensional (2D) or 3D matrices to mimic ligament tissue. As 2D matrices, fibroblast cells are mechanically stimulated by deforming the flexible cell culture dish. Many times 2D fibroblast models are stretched in uniaxial tension to 5% - 8% [28,29] at 1 Hz frequency and have shown increases in cellular proliferation in response to stimulation [14]. However, discrepancies between the behavior of cells in 2D matrices and *in vivo* have encouraged the use of 3D models, which better mimics the micro-environment of living tissue [30]. As 3D models, fibroblasts are typically seeded within scaffolds made of collagen, polyurethane, cellulose, or fibrin gel and tested in

uniaxial tension (0-10%) [31–33] or compression (5%-10%) [13,34]. More importantly, 3D fibroblast models have shown changes in cell proliferation, increases in matrix strength/stiffness, and increases in collagen density when stimulated over time [13,35,36]. One of the main differences between 2D and 3D models is the rate of cell proliferation, where 3D matrices typically display greater cell proliferation [37]. Therefore, the matrix model greatly influences cellular behavior and the rate of tissue remodeling. Overall, the results from 2D and 3D fibroblast matrix studies demonstrate that dynamic loads will increase cellular activity, and thus have the potential to result in improved mechanical integrity of tissue.

2.2 Bioreactors

2.2.1 Purpose

Bioreactors are devices where biological, biochemical, and biomechanical processes are produced within a highly controllable environment. Although bioreactors are commonly utilized in the field of tissue engineering, these apparatuses have also been used in other diverse areas, such as fermentation, water treatment, food processing, and pharmaceuticals [38]. The development of tissue engineering bioreactors progressed from the bioreactors used in the 1980s for animal cell culture, where they were needed to develop vaccines and culture large cell populations [39]. Today, tissue engineering bioreactors have been designed to mimic the mechanical and biological environment of natural soft tissues, such as ligaments, to better identify treatments that accelerate and strengthen tissue healing. Thus, the development of tissue engineering bioreactors can allow for controlled mechanical loads to be applied to tissue-like constructs to understand the optimal loads that encourage cell remodeling. In order to produce a controllable

environment for the study of certain processes, tissue engineering bioreactors typically include an actuating system and culture chamber, which provides the mechanical stimulation and controlled biological environment, respectively. More advanced tissue engineering bioreactors may also implement medium circulation structures, monitoring networks, or feedback systems.

2.2.2 Types of tissue engineering bioreactors

Tissue engineering bioreactors can be categorized based on the type of applied mechanical forces, such as hydrodynamic shear, uniaxial loads, equibaxial loads, or biaxial loads. Spinner flask and rotating vessel bioreactor systems use continuous stirring of the culture medium to provide nutrients to the tissue constructs as well as provide hydrodynamic shear forces [39–41] (**Fig. 2A,B**). In spinner flasks, the scaffolds are fixed within the culture chamber while the scaffolds are suspended in rotating vessels bioreactors (**Fig. 2A**). Nonetheless, the conditions in these bioreactors do not accurately represent the tissue environment. Uniaxial bioreactors apply either dynamic tensile or compressive loads along one preferred axis to tissue constructs [13,15,17] (**Fig. 2C)**. These systems provide mechanical loads at physiological frequencies during cell culture to stimulate cellular activity and tissue remodeling. However, uniaxial bioreactors are limited in applying loads to only one axis. For this reason, equibiaxial or biaxial bioreactors have been recently developed to subject tissue constructs to loading conditions along two axes, which better mimics the physiological loading environment of tissue (**Fig. 2D,E**). Equibiaxial bioreactors primarily consist of applying tensile stretch to cruciform-shaped constructs [42,43] while biaxial systems simultaneously apply compressive and tensile loads [44]. With tensile and compressive loads, biaxial

bioreactors can produce states of material distortion, which has been shown to be an excellent predictor of failure in ductile materials [45]. However, the impact of material distortion or volume change to promote fibroblast activity and tissue remodeling remains unclear.

2.3 Continuum Mechanics

2.3.1 The mechanics of applied loads – deviatoric and dilational

Figure 2 Types of tissue engineering bioreactors. A) Spinner flask, B) Rotating vessel, C) Uniaxial, D) Equibiaxial, and E) Biaxial bioreactor systems.

Currently, fibroblast activity is evaluated based on their response to a specific magnitude of strain applied in one axis. However, this method does not consider or measure the stress states being applied to the tissue construct. Therefore, the loading conditions applied by tissue engineering bioreactors should be collected and quantified as stress and strain components. Furthermore, any stress or strain tensor can be expressed as deviatoric (distortion) and dilational (hydrostatic) components (Eq. 1-4). Deviatoric components produce a change in material shape at a constant volume, while dilational creates a change in material volume at a constant shape. Simply put, deviatoric relates to material distortion and dilational relates to volume change. More importantly, distortion causes shearing in materials, but volumetric changes do not. Together, deviatoric and dilational components equate to the original tensor (**Fig. 3**).

$$\boldsymbol{\sigma_{dil}} = \frac{1}{3}(\boldsymbol{\sigma_{xx}} + \boldsymbol{\sigma_{yy}} + \boldsymbol{\sigma_{zz}}) \quad (1)$$

$$\boldsymbol{\sigma_{dev}} = \boldsymbol{\sigma_{total}} - \boldsymbol{\sigma_{dev}} \quad (2)$$

$$\boldsymbol{\varepsilon_{dil}} = \frac{1}{3}(\boldsymbol{\varepsilon_{xx}} + \boldsymbol{\varepsilon_{yy}} + \boldsymbol{\varepsilon_{zz}}) \quad (3)$$

$$\boldsymbol{\varepsilon_{dev}} = \boldsymbol{\varepsilon_{total}} - \boldsymbol{\varepsilon_{dev}} \quad (4)$$

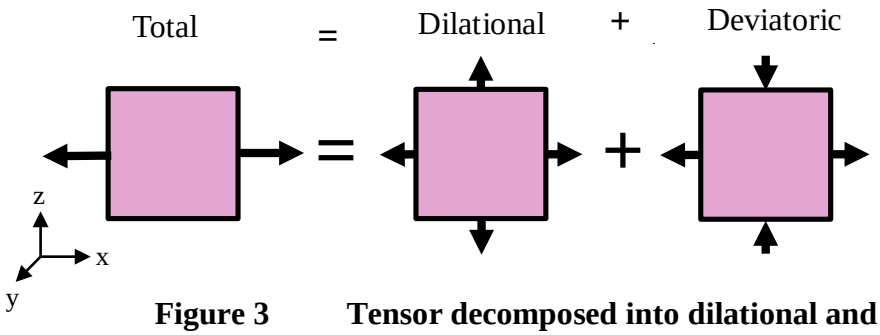

Figure 3 Tensor decomposed into dilational and deviatoric components.

2.3.2 Strain energy density in literature

Strain energy is defined as the potential energy stored in an elastic material due to deformation while strain energy density has been normalized by accounting for the volume of the material. Strain energy as a parameter has allowed for the development of hyperelastic constitutive models, which are used to model materials that respond elastically when subjected to very large strains. More specifically, the constitutive law for a hyperelastic material is defined by an equation connecting free energy of a material to the deformation gradient. However, most constitutive laws implement strain energy density as opposed to free energy to avoid introducing mass density in the stress-strain relations. An example of a hyperelastic material model is the Ogden, where the strain energy density function is expressed in terms of the principal stretches of the material.

Other hyperelastic models include Mooney-Rivlin and Neo-Hookean, where each has a different strain energy density function.

In addition to constitutive modeling, energy to failure, a parameter similar to strain energy density, has been experimentally measured in conventional as well as biological materials. Energy to failure, which is defined as the area under the load-deformation curve until complete failure, has been calculated for fiber-reinforced composites to understand how materials fail on impact [46]. Energy to failure is also a common parameter for understanding the failure mode of high strength steel and carbon spot welds [47,48]. For biological materials, this parameter is often used to determine the relationship between energy absorption and the state of failure for anterior cruciate ligaments [49]. Furthermore, it is also used to investigate the biomechanical integrity of intact and healing Achilles tendon [50] as well as evaluate the role of the knee meniscus in energy absorption of the knee [51]. Overall, the measurement of energy to failure has allowed previous studies to assess how energy is absorbed or dissipated in materials until reaching failure.

Other studies have successfully quantified and varied strain energy density within soft tissue, but have yet to control or measure local strain energy density within a material. In Snedeker et al., strain energy density was experimentally calculated as the kinetic impact energy divided by the volume of the organ, where kinetic impact energy was calculated as the energy transferred from a polyamide ball to the organ [52]. To examine organ failure at higher impact velocities, the polyamide ball was fired between 1-25 m/s. This range of velocities corresponded to a strain energy density failure range of 20-30 kJ/m^3. Another organ injury study calculated strain energy density for compressive

failure tests at different strain rates (0.005 s^{-1}, 0.05 s^{-1}, 0.5 s^{-1}). Strain energy density was then calculated as the integral of stress with respect to strain to the ultimate failure strain. Similar to Snedeker et al, the strain energy density of the organs was reported to be between 18-33 kJ/m^3. Even though these studies determined and varied the amount of strain energy density being applied to organs, they did not control nor locally quantify the total strain energy density within the material. Furthermore, the distortion or hydrostatic energy of organ failure was not measured or reported, which would have been a valuable parameter to help understand the type of energy that caused organ failure. Distortion energy theory, which states that material failure will occur due to distortion or shear and not due to hydrostatic or volume change, is typically implemented in finite element models to assess the mode of failure [53,54]. However, to our knowledge, distortion energy has not been experimentally measured in soft tissue. Therefore, an innovative approach would be to control the total strain energy in order to measure the distortion and hydrostatic energy to fully understand the specific impact of these energies on cell response.

2.3.3 Distortion and hydrostatic energy

Similar to stress and strain, strain energy density can be decomposed into distortion and hydrostatic components (Eq. 5).

$$W = \int \boldsymbol{\sigma}(\boldsymbol{\varepsilon})\, d\boldsymbol{\varepsilon}_{dev} + \int \boldsymbol{\sigma}(\boldsymbol{\varepsilon})\, d\boldsymbol{\varepsilon}_{hydro} \qquad (5)$$

Distortion has been shown to alter the function of non-biological and biological materials. In fact, the distortion energy theory is an excellent predictor of ductile material failure [45]. This theory states that yielding will occur when the distortion energy reaches the point that equates to yielding in a simple tension test. Thus, yielding is strictly

independent of hydrostatic stresses and relies purely on distortional stresses. Because distortion causes shearing, this theory implies that failure in ductile materials is due to only shear.

Several previous studies have applied shear stresses through sliding contact to 3D cell-seeded scaffolds and have reported improved tensile properties, alterations in collagen content, and increased cell proliferation [55,56]. The findings of these studies suggest that distortion energy governs cellular response. Yet, the levels of applied distortion were not quantified and these systems only applied shear to the construct surface as opposed to the bulk of the material volume. Therefore, a need exists to use a novel bioreactor system that can apply uniform stresses to the bulk of a construct in order to develop an experimental methodology that can apply varying levels of distortion, while maintaining a constant strain energy density, to understand how distortion specifically influences the cellular activity, matrix structure, and mechanical function of cellularized constructs.

CHAPTER THREE: QUANTIFYING DISTORTION ENERGY IN 3D CELLULAR COLLAGEN CONSTRUCTS SUBJECTED TO COMPLEX LOADS USING A BIOREACTOR

3.1 Introduction

Mechanical loads stimulate the growth and remodeling of collagen networks by fibroblasts in musculoskeletal soft tissues, such as ligament and tendon [14,57]. To understand how fibroblasts respond to specific loads, studies have subjected 3D cellularized constructs to physiological relevant forces in tension, compression, and shear [13,15,16,27]. These studies have revealed that fibroblast-mediated collagen production is regulated by mechanical stimulation, such as simple and complex loads, applied to the extracellular matrix [58]. Even though these studies have identified certain loading conditions that are beneficial or detrimental to cell activity [13,16,27,59], there is no unifying theory that can predict fibroblast response for any type of loading configuration (i.e. tension, compression, planar, 3D). The potential to predict extracellular matrix deformation on collagen network remodeling and repair would have positive outcomes in connective tissue physiology, tissue engineering, and musculoskeletal medicine. This would also include the physical rehabilitation of tendon and ligament injuries.

A potential solution to help develop a unified theory to predict fibroblast response is to quantify applied mechanical forces to 3D cellular constructs in terms of strain energy density. Strain energy density is the stored energy due to material deformation and can be decomposed into distortion (deviatoric) and hydrostatic (dilational) energy.

Distortion energy causes a change in material shape, without affecting the material volume; while hydrostatic energy causes a change in material volume, without affecting the material shape. Therefore, measuring strain energy density can identify the physical changes that primarily govern cell activity. Researchers have commonly observed that distortion energy alters the function of non-biological and biological materials. For example, distortion energy theory is an excellent predictor of failure in ductile materials [45]. Currently, strain energy density has been experimentally measured in biological tissues, such as during the impact testing of organs [52]. Distortion energy theory has been used in finite element models to evaluate failure in materials, such as bone [53,54], but has yet to be experimentally measured or varied within a biological material. A major limiting factor in conducting experiments to study the effect of distortion energy on cell activity is that there is no established methodology to apply controlled levels of strain energy density to 3D cellular constructs.

One potential approach to overcome this limitation is to simultaneously apply tension and compression to 3D constructs. By varying the magnitudes of compression and tension, it is possible to apply different amounts of distortion energy, while maintaining the total strain energy density being applied to the construct. The validation of this novel approach would enable researchers to differentiate and model the effects of distortion energy and hydrostatic energy on fibroblast mechanotransduction.

The objective of this research was to develop and validate a new experimental method to subject 3D collagen constructs to differing magnitudes of distortion energy while maintaining a targeted strain energy density. The accuracy of this method was quantified in both non-cellularized and cellularized collagen constructs.

3.2 Materials and Methods

3.2.1 Overview

A custom biaxial bioreactor was developed to apply tensile and compressive forces used to mechanically stimulate 3D constructs as well as measure strain fields as the constructs deformed. This bioreactor was then used to apply a targeted strain energy density while differing the amounts of distortion during various loading conditions.

3.2.2 Bioreactor design

The custom bioreactor consisted of a tension and compression assembly, a culture chamber to contain the collagen specimens with cell media, and a camera housed at the base of the bioreactor for specimen strain tracking (**Fig. 4**). The primary mechanical components of the bioreactor were constructed from stainless steel, acrylic, or clear polycarbonate, since these materials could withstand the warm incubator environment as well as ethanol and ultra-violet light sterilization techniques. Additionally, the overall design of the bioreactor was developed to fit within the confines of an incubator.

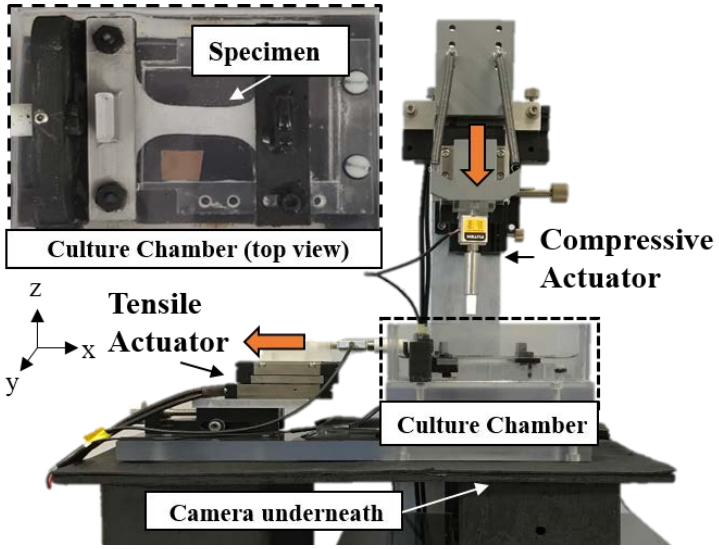

Figure 4 Primary components of the biaxial bioreactor include the compressive and tensile actuators, culture chamber, and camera. Specimens were placed in the culture chamber for mechanical stimulation.

The tension and compression assemblies were developed to apply mechanical stimulation to cellularized constructs. More specifically, the assemblies used high precision voice coil actuators (SLA-25-010-55-1, SMAC, Carlsbad, CA) due to no backlash and minimal wear overtime. The actuators were powered with a 24 V power supply (Keysight E3631A) and connected to 2 single-axis amplifiers (LAA-5, SMAC, Carlsbad, CA). The specifications of the actuators include having a 10 mm stroke, 4 N force output, and being equipped with 1 μm linear encoders. For the tension assembly, a force sensor (LAA-5, SMAC, Carlsbad, CA) connected to the end of the actuator with a tensile grip was used to clamp and record the loads applied to one end of the specimen. Force measurements were then recorded using a four channel NI9269 strain gauge module. The tensile shaft, which joined the force sensor to the tensile grip, was connected through the wall of the culture chamber. Within the culture chamber, a clear polycarbonate tissue platform with four fixed-position threaded holes allowed specimens

between 10 to 40 mm long to rest and be clamped on the other end with another tensile grip (**Fig. 4**). The tensile grips, adhered with 50 grit sandpaper, directly compressed the ends of the specimen either between the platform and another grip or between two grips. All grips were securely fastened with nylon screws and nuts. Lastly, the tensile actuator was rigidly connected to a horizontal translator, which allowed flexibility in positioning the grip relative to the specimen. For the compression assembly, a force sensor with a ~6 x 6 x 3 mm Teflon loading platen was used to apply and record compressive loads to the specimen. The compression actuator was rigidly connected to a two-axis translator, allowing the compressive loading platen to move relative to the specimen position. A clear polycarbonate base plate was also used to hold both the assemblies and culture chamber.

Force and displacement were regulated and evaluated, respectively, by the tension and compression actuators, which were controlled using a Compact-Rio 9024 and two NI9514 servo interface drives (National Instruments, Austin, TX). A user can operate the bioreactor through a custom LabVIEW software (National Instruments, Austin, TX) installed on a dedicated PC. The software uses a force feedback control loop to dynamically regulate the position command sent to the actuators. In detail, the force-controlled stimulation is initiated by sending synchronized sinusoidal waveforms for tension and compression at user-specified displacements to each actuator. Furthermore, the program is able to monitor the maximum and minimum peak forces for each force waveforms and shift the respective position waveforms until the forces register within a user-specified threshold.

A camera (Apple, Cupertino, CA; 12 MP camera with 30 fps) was positioned directly under the culture chamber for digital imaging correlation (DIC), which was implemented to measure and track the strain fields of the collagen construct during testing (**Fig. 4**). Because of the implementation of clear polycarbonate components, a specimen could easily be viewed and recorded during testing. Additionally, a stand was developed to hold the bioreactor a set distance of 34 inches from the camera, which was necessary to clearly focus on the specimen. For lighting, two light strips were adhered under the base of the culture chamber. Furthermore, black covered lids were placed on top of the culture chamber to help contain the light.

3.2.3 Experimental procedure to measure distortion energy

A procedure was developed to use the biaxial bioreactor to apply differing levels of distortion energy while controlling the total strain energy density to 3D collagen constructs. For this study, five different loading conditions were selected to vary the levels of distortion energy applied to the constructs and a constant total strain energy density was chosen by the user. To investigate the impact of cells on distortion energy, non-cellularized constructs were tested first and then later cellularized, where both followed the same testing procedure. The procedure to measure distortion energy can be broken down into four main steps: construct preparation, bioreactor testing, strain tracking, and data analysis with validation.

To prepare the constructs, type-I collagen sponges (n = 5; DSM, Exton, PA) were cut into a dog-bone shaped geometry using a custom designed punch and speckled with water insoluble black ink using a commercially available DIC stamp (**Fig. 5;** Correlated Solutions, Irmo, SC).

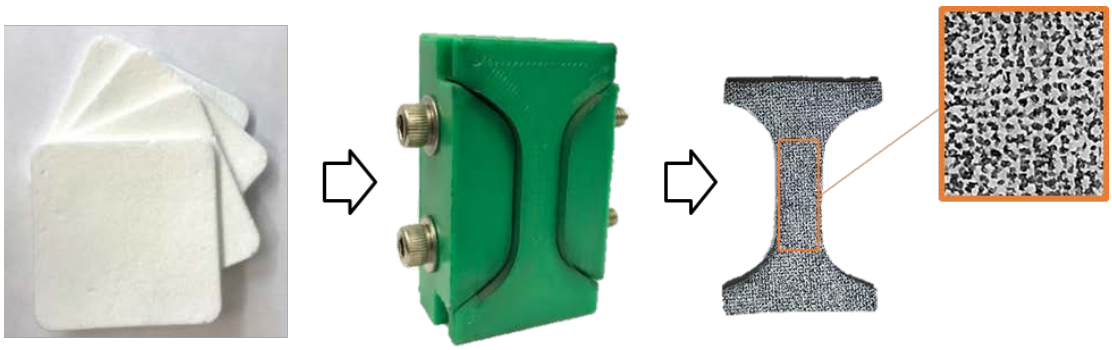

Figure 5 Construct preparation. Type-I collagen sponges were first punched into dog-bone shaped geometry and then speckled with black ink using a DIC stamp.

To fully hydrate, the constructs were soaked in water for 2 hrs. Once hydrated, the constructs were placed in the culture chamber, where both tabs were clamped down by the adjustable grips and construct dimensions were measured. In addition, friction was reduced between the tissue platform of the bioreactor and the specimen interface by applying a clear, biocompatible lubricant (Miller-Stephenson Chemical Company, Danbury, CT). For the medium, water was added to fill the tissue chamber.

For bioreactor testing, the constructs were subjected to 5 different loading conditions: only tension (*T*), only compression (*C*), equal tension and compression (*T/C*), compression with low magnitudes of tension (*LT/C*), and tension with low magnitudes of compression (*T/LC*). Furthermore, all loading conditions were stimulated to and analyzed at 500, 1000, and 2000 cycles. To reach the maximum stimulation cycle, the constructs underwent 30 minutes of mechanical testing, where previous studies typically stimulate from 30 minutes to 1 hour [60–62]. Prior to testing, the constructs were preloaded to 0.05 N in tension and 0.015 N in compression, depending on the loading condition. Second, the user selected a targeted strain energy density for a localized region of the construct to be used for all loading conditions. For this study, the user-selected targeted strain energy density was set to 300 J/m^3, which corresponded to tensile and compressive forces that did not cause material damage to the collagen constructs. In general, the procedure to measure strain energy density in the collagen constructs consisted of two main steps: 1)

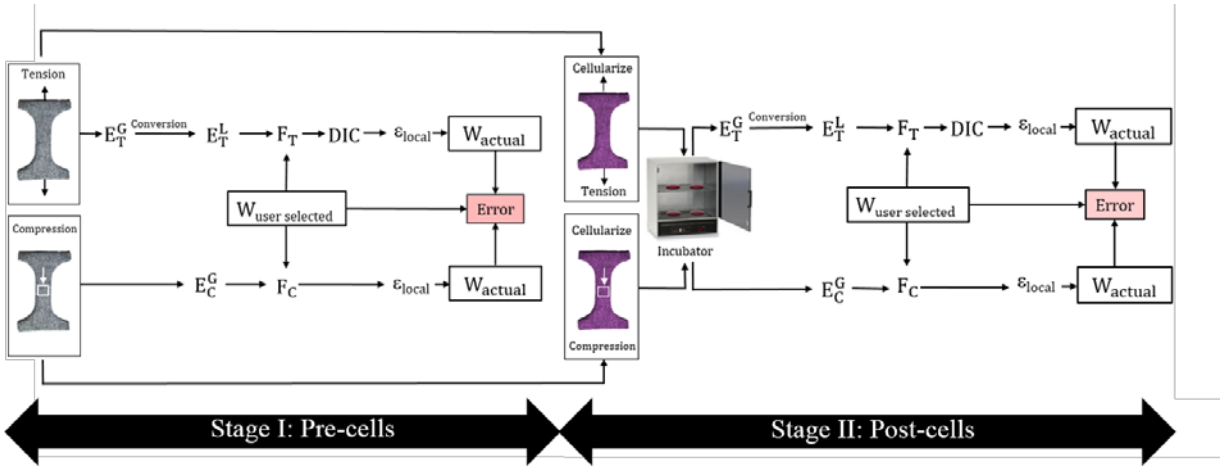

Figure 6 Flow chart of the bioreactor testing methodology to measure strain energy density. Elastic moduli for tension and compression were determined and used to calculate the forces to achieve a user-selected strain energy density. The actual strain energy density was computed from synced stress data from the bioreactor and strain data from DIC. The percent error between the user-selected and actual strain energy density provided the accuracy of this methodology for non-cellularized and cellularized constructs.

determining the local elastic moduli to find the forces that correspond to the targeted strain energy density and 2) calculating strain energy density using the local engineering strains and engineering stresses (**Fig. 6**).

The equation for strain energy density, *W*, is equal to area under the stress-strain curve (Eq. 6, left). More specifically, engineering stress, σ, and global engineering strain, ε_g, were computed along the x- and z-axes using the force sensor data of the entire construct. Local engineering strain, ε_l, was converted from Green-Lagrange strain along the x- and y-axes by tracking the construct speckle patterns using DIC in a region of interest (ROI) (**Fig. 7**).

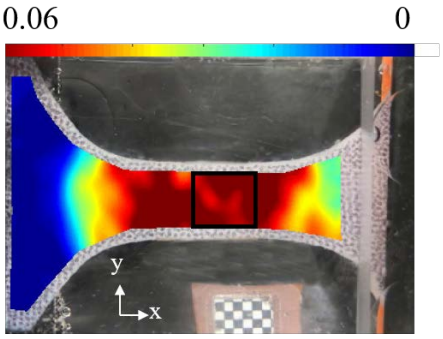

Figure 7 Representative DIC colorimetric map of Green-Lagrange strain for the only tension group (black line = ROI).

Because the bioreactor operates in force control, tensile and compressive forces had to be calculated to apply the user-selected total strain energy density, where this relationship is also dependent on specimen area, *A*, and local elastic modulus, *E* (Eq. 6, right).

$$W = \int \boldsymbol{\sigma}(\boldsymbol{\varepsilon_l})\, d\boldsymbol{\varepsilon} \rightarrow F = A\sqrt{2WE} \qquad (6)$$

Therefore, the local tensile and compressive elastic moduli of the constructs had to be determined in order to input the tensile and compressive forces into the bioreactor corresponding to the 5 loading conditions (**Fig. 6**).

To calculate the local elastic moduli, the samples were independently stimulated in tension and compression to 300 cycles, which is the number of cycles necessary to achieve equilibrium, until obtaining forces that gave an error of less than 10% between the actual and user selected strain energy density of 300 J/m^3. The global strains from the only tension test were then converted to local strains using a linear regression equation, which was determined from non-cellularized constructs (**Fig. 8A**). The local tensile elastic modulus was determined by calculating the area under the actual stress-converted local strain plot, finding the corresponding maximum stress and strain for this area as a linear fit, and then computing the slope of this fit (**Fig. 8B**).

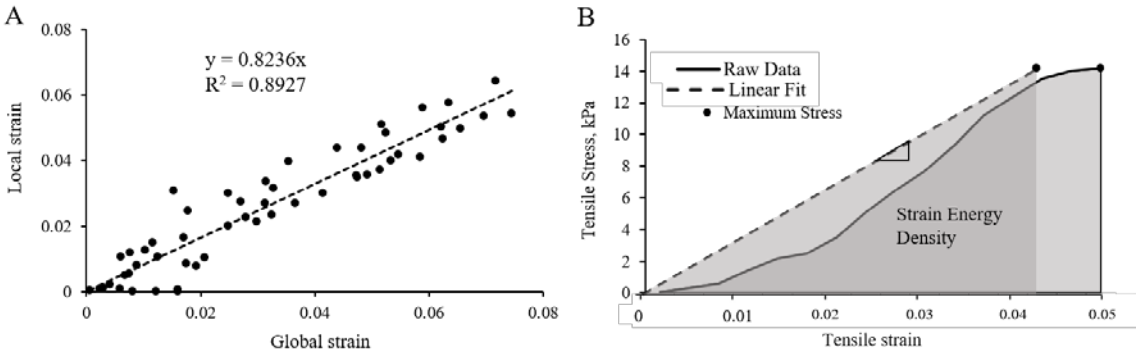

Figure 8 Plots to calculate the local tensile elastic moduli. A) Conversion of global strains to local strains using the regression equation. B) Representative stress-strain plot and linear data fit.

The local compressive elastic modulus was calculated using the same approach as tension, but global strain was used since the ROI on the construct was the same for local and global states. This process was iterative to ensure accurate tensile and compressive elastic moduli of the specimens, which was crucial in successfully calculating the forces for all loading conditions to achieve the user-selected total strain energy density (Eq. 6, right) . For the combined loading *T/C* group, the determined tensile modulus and compressive modulus were used to select tensile and compressive forces that each

applied half of the total targeted strain energy density. In addition, the tensile and compressive forces for the *T/LC* group were selected to equal 2/3 and 1/3 of the total targeted strain energy density, respectively. Similar calculations were then conducted for the *LT/C* group.

To determine the local engineering strains to calculate strain energy density, strain tracking of the construct was completed through Ncorr, an open source DIC MATLAB software (MathWorks Inc., Natick, MA). This program was able to measure and track the construct speckle pattern to calculate the local engineering strain in the construct ROI. In order to sync the stress data from the bioreactor and strain data from the camera at selected cycles, an automated LED was programmed into the LabVIEW software. Furthermore, a calibration square that consisted of 1 x 1 mm black and white squares was placed next to the prepared constructs in the culture chamber to accurately calculate construct displacement and strain (**Fig. 7**). To find the local engineering strains, the video recorded from the camera was first imported into Photoshop (Adobe, San Jose, CA) to convert to images at the camera's frame rate. Second, ImageJ (NIH, Rockville, MD) was used to crop and re-orient the images necessary for Ncorr. Third, the images were imported into Ncorr from the starting position to maximum displacement of specific cycles. The Green-Lagrange strains were computed for the entire construct with all parameters set at default. The calibration square was also selected to ensure accuracy in the measured displacement and strains. Lastly, a custom Matlab script was written to convert Green-Lagrange strain to local engineering strains within the ROI.

During data analysis and validation, the strain energy density for specific cycles for all loading conditions was calculated and compared to the user-selected total strain

energy density (**Fig. 6**). Using Matlab, a custom script was developed to calculate strain energy density as incremental areas under the non-linear engineering stress-local engineering strain plot. First, the stress and strain data were organized into individual tensors. Then, any noise in the stress and strain data was manually removed, which was defined as negative tensile stresses and decreasing compressive strains during testing. Second, the changes in stress and strain were computed at each strain interval. Third, the deviatoric and hydrostatic components were calculated for each change in stress or strain (Eq. 7-10). Fourth, the deviatoric and hydrostatic components for stress and strain were used to calculate the non-linear area as incremental rectangle and triangles, which is equal to the total strain energy density (Eq. 11). For validation, the developed code was compared to the area values generated by the trapezoidal numerical integration function. In addition, sample cases of pure hydrostatic and pure deviatoric states were used to confirm the correct calculation of hydrostatic and deviatoric terms. Percent error was determined between the actual strain energy density and the user-selected strain energy density for all loading conditions at specific cycles. The same constructs were then cellularized and subjected to the aforementioned bioreactor testing procedure (**Fig. 6**).

$$\Delta\boldsymbol{\sigma}^{hydro} = \frac{1}{3} tr(\Delta\boldsymbol{\sigma})\boldsymbol{I} \quad (7)$$

$$\Delta\boldsymbol{\sigma}^{dev} = \Delta\boldsymbol{\sigma} - \Delta\boldsymbol{\sigma}^{hydro} \quad (8)$$

$$\Delta\boldsymbol{\varepsilon}^{hydro} = \frac{1}{3} tr(\Delta\boldsymbol{\varepsilon})\boldsymbol{I} \quad (9)$$

$$\Delta\boldsymbol{\varepsilon}^{dev} = \Delta\boldsymbol{\varepsilon} - \Delta\boldsymbol{\varepsilon}^{hydro} \quad (10)$$

$$W = \left[(\Delta\boldsymbol{\sigma}:\Delta\boldsymbol{\varepsilon})_{rec} + \frac{1}{2}(\Delta\boldsymbol{\sigma}:\Delta\boldsymbol{\varepsilon})_{tri}\right]_{dev} + \left[(\Delta\boldsymbol{\sigma}:\Delta\boldsymbol{\varepsilon})_{rec} + \frac{1}{2}(\Delta\boldsymbol{\sigma}:\Delta\boldsymbol{\varepsilon})_{tri}\right]_{hydro} \quad (11)$$

3.2.4 Preparation of cellularized specimens

Before bioreactor testing, the non-cellularized constructs underwent a strict sterilization and cell seeding process. First, the constructs were saturated in 70% ethanol and then allowed to completely dry inside a biosafety cabinet (Labconco, Fort Scott, KS). Second, ultra-violet light was then applied for 10 minutes on each construct side to ensure complete sterilization. Third, the constructs were hydrated with 1-2 ml of growth medium (high-glucose Dulbecco's Modified Eagle's Medium with 10% bovine calf serum and 1% penicillin-streptomycin) and placed within a sterilized, 3D-printed specimen mold inside a petri dish. In detail, the specimen mold was used to ensure cell adhesion to the collagen construct opposed to the dish directly and vacuum grease (High Vacuum Grease, Dow Corning, Midland, MI) was applied to the bottom of the mold to contain the cell media. The constructs were then seeded with NIH/3T3 fibroblast cells (ATCC® CRL1658™) at a density of ~10^6 cells/construct, which was a similar concentration of cells used to seed tissue constructs in previous studies [43,60,63,64]. Lastly, the constructs were allowed to statically culture for 2 days in a humidified incubator (VWR, Radnor, PA, 37.1°C, 5% CO2) to ensure complete cellular permeation of the collagen foam and then mechanically tested in the bioreactor. Thus, there were two different construct types, non-cellular and cellular, where the cellular constructs were included to investigate the influence of remodeled constructs on distortion energy. Overall, the goal of these methods with non-cellular and cellular constructs was to prepare for future studies that will include cellular constructs undergoing mechanical stimulation using the bioreactor within an incubator.

3.2.5 Cell viability assay

To ensure that the experimental protocol did not accelerate cell death, a CellTiter 96® Aqueous Non-Radioactive Cell Proliferation Assay (MTT assay; Promega, Madison, WI) was conducted on fibroblast-seeded collagen sponges, which is a common procedure to determine cell viability in tissue-like constructs [60,65]. The MTT assay is a standard colorimetric assay for evaluating cell metabolic activity, where mitochondrial enzymes reduce the yellow MTT dye to formazan. First, a standard curve of lives cells in the collagen sponges was correlated to absorbance values. The collagen sponges (n = 16) were punched into 12.7 mm diameter by ~2 mm thick plugs and subjected to the sterilization process, which included saturating in 70% ethanol, allowing to completely dry, and applying ultra-violet light for 10 minutes. A 24-well plate was then prepared with the fibroblast-seeded collagen plugs and cell media for a total volume of 1000 µL. In the 24-well plate, each column contained a concentration of cells from 250,000 to 41,667 with a decreasing interval of 41,667 cells. The cells were then allowed to adhere for 48 hours within each well. After this time, 150 µL of the provided Dye Solution was added to each well and the plate was set in an incubator for 3 hrs. Following incubation, 1000 µL of the Solubilization Solution was mixed into each well and the plate was allowed to incubate for 1 hr. The contents in each well, except for the collagen plugs, were then transferred to a new 24-well plate, where each well was mixed until a uniform color was achieved. The absorbance of the plate was measured and recorded at a test wavelength of 570 nm and a reference wavelength of 690 nm using a plate reader (Synergy H1 Hybrid Multi-Mode Plate Reader, BioTek Winooski, VT). The reference absorbance was subtracted from the test absorbance in order to remove any background

interference, such as cell debris. The absorbance values were then correlated to the known cell count, allowing a standard curve to be determined of live cells in the collagen foams (**Fig. 9**). Second, the standard curve was then used to determine the cell viability in fibroblast-seeded collagen plugs that followed the same construct preparation process as the mechanically stimulated group. For these collagen plugs (n = 2) to be similar to the mechanically stimulated group, they underwent the same total hydration time in water, bioreactor tissue culture environment, sterilization procedure, cell seeding methods, and incubation time. For cell seeding, each collagen plug was seeded with 187,112 cells, which was calculated based on the ratio of scaffold surface area to 10^6 cells. Similar to the mechanically stimulated group, the collagen plugs were allowed to incubate for two days in a 3D-printed specimen mold with vacuum grease. After incubation, the well contents, including the collagen plugs, were transferred to a 24-well plate to prepare for plate reading. These collagen plugs then underwent the same amount of Solubilization and Dye Solution as well as time in incubation as the standard cell curve procedure. Prior to plate reading, the well contents were transferred to a new 24-well plate without the collagen plugs. By having the collagen plugs undergo the exact same protocol as the mechanically stimulated group while the collagen plugs used to create the standard curve did not, the effect of the protocol to prepare the mechanically stimulated group on cell viability became evident. After correlating to the standard curve, the collagen plugs had a cell viability of 96.7%, which suggests that the cell culture protocol prior to mechanical stimulation had minimal influence on cell viability (**Fig. 9**). Overall, the MTT assay was performed to confirm that the experimental protocol prior to mechanical stimulation did not accelerate cell death in cellular constructs.

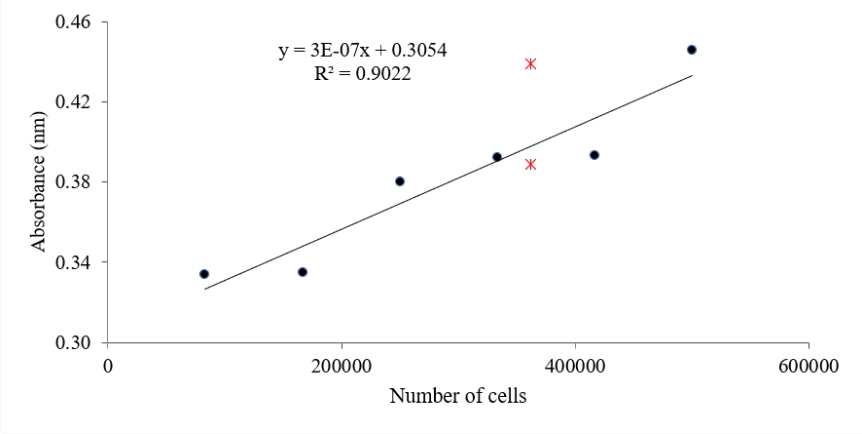

Figure 9 Standard curve to determine cell viability in constructs. Black circles indicate detected cells at the different concentrations. Red asterisks indicate the predicted number of cells in a construct using the standard curve.

3.2.6 Statistical analysis

The effect of loading condition type and duration of stimulation cycles on distortion energy, dilational energy, and percent error in applying a targeted strain energy density was assessed using multiple one-way ANOVAs. Additionally, a Tukey-Kramer adjustment was used for pairwise comparison. A paired sample t-test was also performed to detect differences in distortion energy, dilational energy, and percent error in applying a targeted strain energy density between the non-cellularized and cellularized specimens. For all statistical tests, significant was set at $p < 0.05$.

3.3 Results

The 2D Green-Lagrange strain pattern of all constructs were visualized using DIC (**Fig. 10**). Three out of the five non-celluarized constructs displayed uniform strain fields in the gauge region for all loading conditions (**Fig. 10A**), indicating that friction between the construct and tissue platform was minimal, and did not affect the strain distribution. However, two non-cellularized constructs did exhibit non-uniform strain fields, indicating that tension was not able to completely transfer through the gauge region of the construct when compression was simultaneously applied (**Fig. 10B**). Once the collagen constructs were cellularized, only one of the five constructs had uniform strain fields.

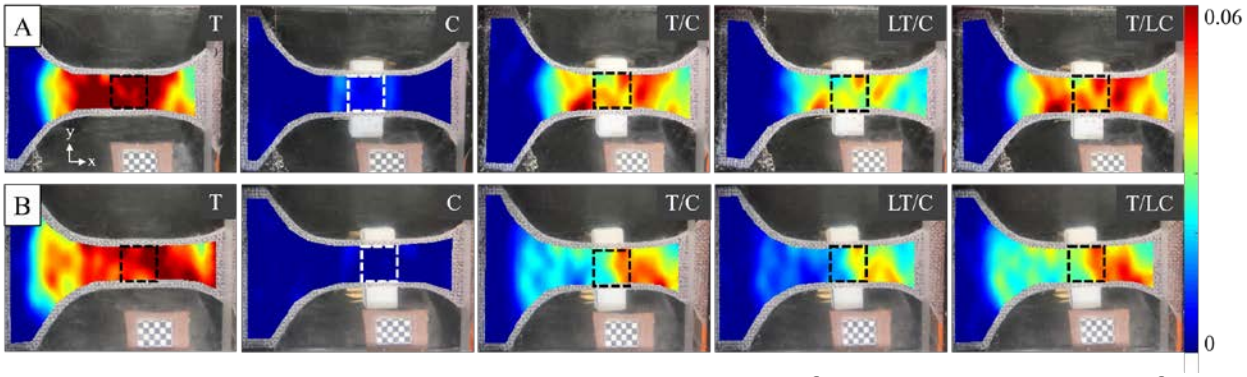

Figure 10 Representative Green-Lagrange strain maps of two collagen constructs for all loading conditions, such as *T, C, T/C, LT/C,* and *T/LC*. Complex loading conditions exhibited either A) uniform strain fields in the x-direction indicating minimal friction between the construct-tissue platform interface or B) non-uniform strain fields indicating friction. Dashed line = ROI.

Distortion and dilational energy were successfully calculated for all specimens within a ROI (**Fig. 10**). Distortion energy calculated for the complex loading conditions experienced an average 308 J/m^3 increase from the simple loading conditions ($p < 0.0005$; **Fig. 11**). Conversely, the dilational energy measured during the simple loading conditions to the complex loading conditions had an average 309 J/m^3 decrease ($p < 0.0005$). Overall, the type of loading condition had a significant effect on distortion and dilational energy ($p < 0.0005$); however, there was no significant difference of distortion and dilational energy between complex loads ($p > 0.339$ and $p > 0.361$, respectively). For example, there was only a 6.9 ± 3.2% difference between the three complex loading conditions for distortion energy. In addition, distortion energy increased 22.1% and dilational energy decreased 42.1% when specimens became cellularized and thus, there was a significant effect of the construct type on distortion and dilational energy ($p <$

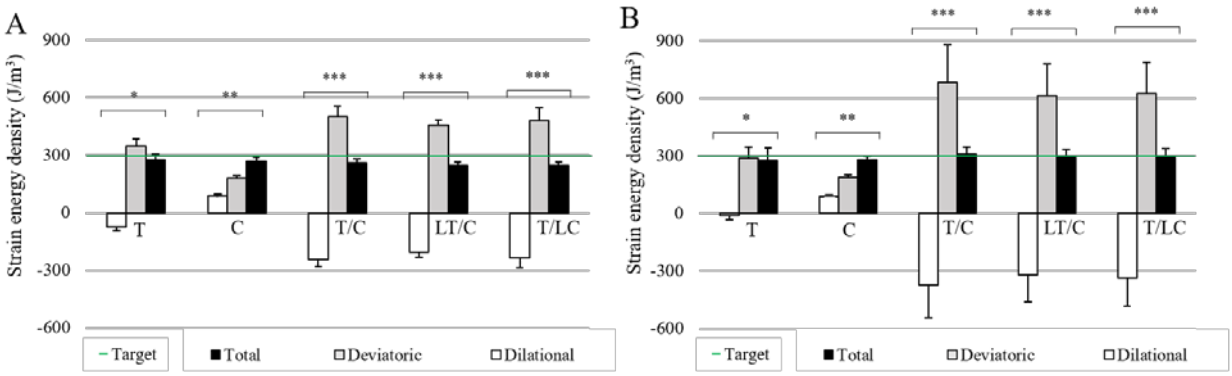

Figure 11 Target and total strain energy density, distortion energy and dilational energy for A) non-cellularized and B) cellularized specimens. One asterisk for the tension group (*) and two asterisks for the compression group (**) indicates dilational and deviatoric energy magnitudes within those groups that are significantly different from all other asterick groups denoting other loading conditions, including between the tension and compression group ($p < 0.0005$). Three asterisks for the combined loading group (***) indicates dilational and deviatoric energy magnitudes within those groups with no significant difference between the loading conditions with the same number of asterisks ($p > 0.339$ and $p > 0.361$, respectively).

0.0005; **Fig. 12**). The duration of stimulation cycles was determined to have no significant effect on distortion or dilational energy (p = 0.952 and 0.995, respectively).

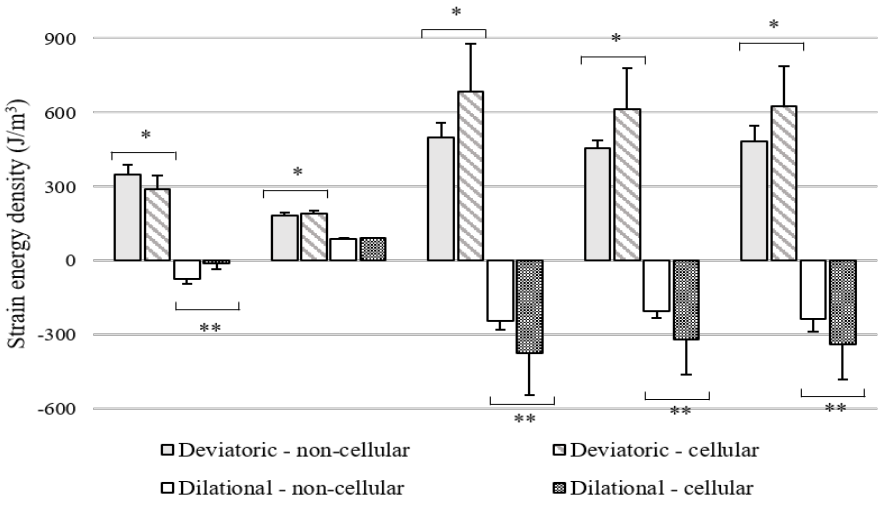

Figure 12 Deviatoric (distortion) energy and dilational energy between construct types. One asterisk (*) and two asterisks (**) indicates significant difference between deviatoric and dilational energy magnitudes between non-cellular and cellular construct group, respectively (p < 0.0005).

The average experimental strain energy density using the bioreactor to apply a targeted strain energy density of 300 J/m^3 for all construct type, loading conditions, and stimulation cycles was 275 ± 39 J/m^3, which corresponded to an average error of 12.7 ± 8.8 % (**Fig. 13)**. There was a 26% increase in average percent error when testing from simple to complex loading conditions. Additionally, there was an approximate 19% difference between the average percent error for non-cellularized (13.9 ± 7.4%) and cellularized specimens (11.5 ± 9.9%). For stimulation cycles, the average percent error for the 500th cycle to the 2000th cycle increased by approximately 24%. However, the effect of loading conditions, construct type, and stimulation cycles on percent error were not significant (p = 0.051, 0.078, and 0.277, respectively).

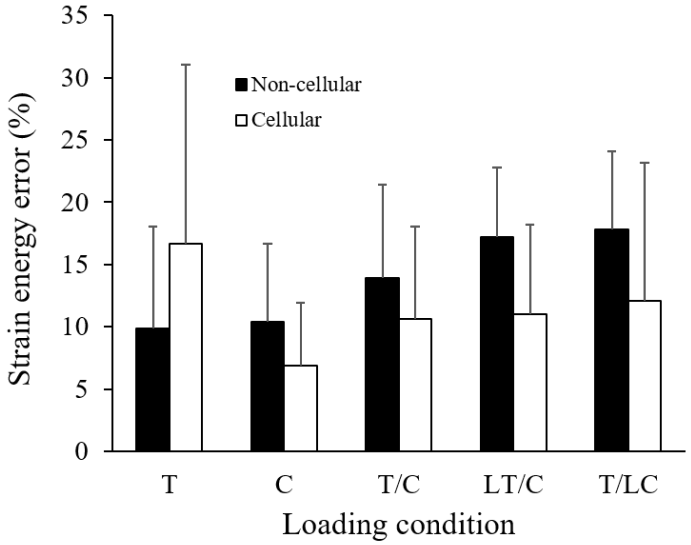

Figure 13 Error in applying the targeted strain energy density of 300 J/m^3 for all loading conditions and construct type. Strain energy error increased from simple to complex loads and decreased from non-cellularized to cellularlized constructs. The effect of loading conditions, construct type, and stimulation cycles on percent error were not significant (p = 0.051, 0.078, and 0.277, respectively).

3.4 Discussion

This study has developed and validated a methodology to measure differing amounts of distortion energy while maintaining a targeted strain energy density in 3D fibroblast-seeded collagen constructs using a novel bioreactor. The procedure described in this study was able to achieve the user-selected targeted strain energy density of 300 J/m^3 with an average percent error of 12.7 ± 8.8 %, where the average percent error for simple and complex loading conditions were 11.0 ± 9.7 %, and 13.8 ± 8.0 %, respectively. Additionally, the average distortion energy was over 2-fold greater for the combined loading condition compared to the simple loads and 22.1% greater when

fibroblast cells were added. These results demonstrate that the novel bioreactor can accurately apply a targeted strain energy density with a low percent error to understand the impact of varying magnitudes of distortion energy on cell response.

To our knowledge, this is the first experimental study to control the total strain energy density in a localized region of a 3D construct as well as measure the distortion energy in 3D constructs. Typically, strain energy density is used to formulate hyperelastic constitutive models, such as Mooney-Rivlin and Ogden, or is used as a criterion to predict crack growth in materials [66]. Strain energy density has also been experimentally measured in biological tissues, such as during the impact testing of organs [52]. These previous studies calculated strain energy density of the organs as the kinetic energy transferred from the impact testing apparatus divided by the mass of the organ. While this technique is practical, it does not account for any energy dissipation, such as heat or sound, that could have decreased the actual strain energy density within the organ. Additionally, even though these previous studies did vary the magnitudes of strain energy density to understand approximately when organs fail, they did not attempt to control a constant amount of strain energy density the organs experienced. More commonly, strain energy is calculated from stress-strain curves to estimate energy to failure [49–51]. Furthermore, energy to failure is measured to understand the relationships between energy and other factors, like material failure or mechanical properties, but has yet to be controlled in research. In this present study, the total strain energy density was experimentally measured and controlled for different loading conditions, construct types, and duration of stimulation cycles.

The biaxial bioreactor was able to successfully apply and control a targeted strain energy density in 3D constructs with a low average error of 12.7%. The experimental procedure used a regression equation (**Fig. 8A**) to convert from global to local strains to predict the local tensile elastic modulus. There was a 16.2 ± 18.0 % error between the converted and actual local elastic modulus for tension. These results demonstrate the feasibility of using a converted local elastic modulus for tension instead of using DIC techniques to determine the actual local elastic modulus. This approach would allow future studies to use the bioreactor to mechanical stimulate 3D cellular constructs within an incubator with moderate accuracy. If the global strains had not been converted to local strains, DIC techniques would have to be implemented, which would be challenging for a few reasons. First, using DIC techniques inside the warm, humid environment of the incubator would impact the performance of the camera needed for this method, such as causing the clear components of the bioreactor to become foggy and interfere with strain tracking of the constructs. Second, an iterative approach would be required for DIC to determine the actual local elastic modulus for tension needed to achieve a targeted strain energy density. This method would be time intensive as the aforementioned procedure to determine the converted local tensile elastic modulus without DIC had 7-8 iterations to achieve the targeted strain energy density with error less than 10%. Thus, including DIC for every iteration would greatly delay the process of determining the elastic modulus for tension. Overall, this study demonstrated that the method of using a regression equation to determine the converted local elastic modulus for tension was practical and future studies can now use this method to successfully run experiments within an incubator.

In this study, the average error between the targeted and actual strain energy density for simple loading conditions was 11.0 ± 9.7 % compared to 13.8 ± 8.0 % for the complex loading conditions. This suggests that the procedure to determine the tensile and compressive elastic moduli were accurate to achieve the targeted strain energy density for the simple loads, but less so for the complex loads. The procedure may not be able to predict the tensile and compressive elastic moduli for complex loads because it did not account for the interaction of the elastic moduli on each other. Moreover, there was no significant effect of the different stimulation cycles on total strain energy density ($p = 0.670$), which indicates that the converted local elastic moduli for tension determined at the 300^{th} cycle can used to calculate a tensile force to achieve the targeted strain energy density at any cycle duration.

The development of this experimental procedure allowed for the identification of the loading conditions that produced high distortion energy and the detection of material properties changes between non-cellular and cellular constructs, which may be attributed to the presence of cells. The combined loading conditions had the largest amount of distortion energy compared to the simple loading conditions with an average increase of 307.8 J/m^3 from simple to complex loads (**Fig. 11**; $p < 0.0005$). However, there was little variation in distortion energy between the three types of combined loads, which suggests that distortion is insensitive to varying magnitudes of simultaneously applied tensile and compressive forces. Additionally, the combined loading conditions also had the largest amount of dilational energy with -285.5 ± 123.9 J/m^3 (**Fig. 11**; $p < 0.005$). The only compression loading condition generated positive dilational energy while the other loading conditions were negative. For the only compression loading condition, the

constructs were stressed and strained in the same z-direction, thus the dilational stresses and strains were both positive (**Fig. 14A**). This type of loading configuration then generated a positive dilational energy. In the only tension loading condition, the constructs substantially contracted in the y- and z-directions while expanding in the x-direction. For this case, the dilational stresses were positive, but the dilational strains were negative, which overall created a negative dilational energy (**Fig. 14B**). With the combined loading conditions, the construct expanded in the x-direction due to large tensile stresses while contracting in the z-direction because of large compressive strains. This then created positive dilational stresses and negative dilational strains, which equated to a negative dilational energy (**Fig. 14B**). The physical reason for this negative strain energy was the large difference in compressive and tensile stiffness. The constructs were found to be soft in compression, but relatively stiff in tension.

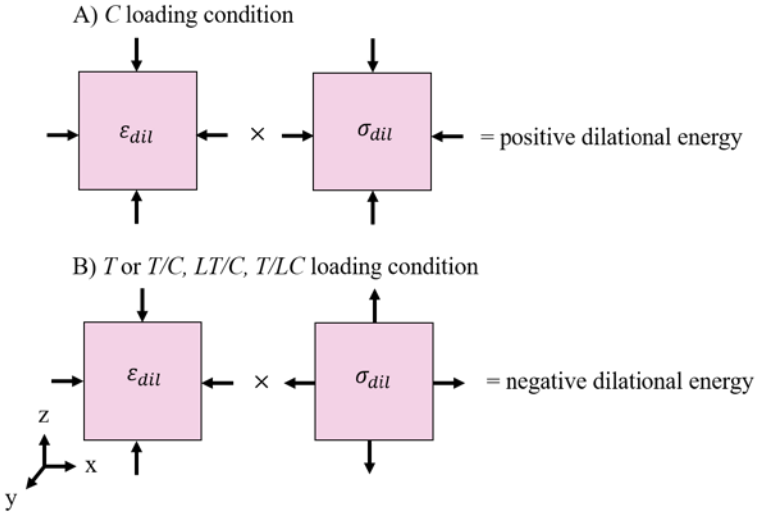

Figure 14 Decomposing each loading condition, A) only compression and B) only tension and complex loads, into stresses and strains to understand type of dilational energy.

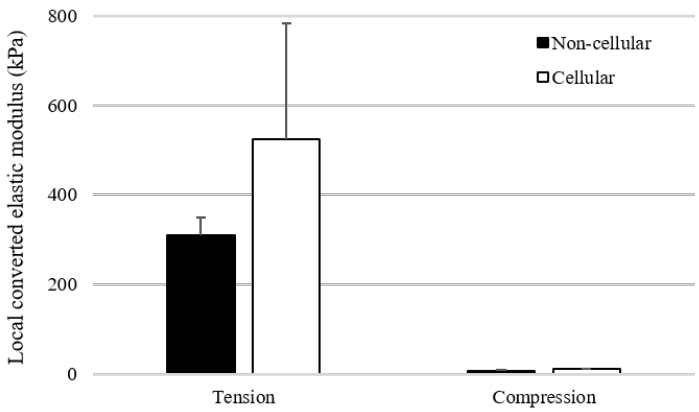

Figure 15 Local converted tensile and compressive elastic moduli in non-cellular and cellular constructs.

For material properties between construct type, the average local converted tensile and compressive elastic moduli determined prior to mechanical testing for non-cellularized were 309.7 ± 40.0 and 7.1 ± 0.8 kPa compared to the cellularized constructs of 523.8 ± 260.3 and 10.1 ± 1.6 kPa (**Fig. 15**). There was an average increase of 17.5% for the tensile elastic modulus and an average decrease of 8.6% for the compressive elastic modulus during the duration of mechanical stimulation for both construct types. Furthermore, there was an average increase of 39.7% and 52.1% for tensile and compressive elastic moduli, respectively, when analyzing the elastic moduli determined from the last loading condition for the non-cellularized constructs to the local converted elastic moduli for the cellularized constructs. This increase in elastic moduli suggest collagen production from the fibroblast cells during the two day incubation period, where collagen content has been shown to be highly correlated with an increase in strength and stiffness in engineered tissues [67,68]. Consequently, this increased stiffness in the cellularized constructs decreased the average percent error between the targeted and actual strain energy density (**Fig. 13**) and may explain the increase in distortion energy between the construct types (**Fig. 11,12**).

The use of DIC techniques to generate colorimetric strain maps enabled the identification of non-uniform strain fields in the x-direction due to friction between the interface of the construct and tissue platform when tension and compression forces were simultaneously applied (**Fig. 10**). To determine the effect of non-uniform strain fields due to friction, the total amount of strain energy density was calculated in the ROI using local stresses and strains, which were then compared to the aforementioned experimental procedure that used global stresses and local strains (**Fig. 6**). For the 500^{th} cycle, there was an average 27 ± 14% decrease in the total strain energy density as a result of the non-uniform strain fields produced by friction during the complex loading conditions. For the constructs with uniform strain fields indicating minimal friction, there was an average 23 ± 9% decrease in the total strain energy density for the complex loading conditions. Overall, there was no significant effect of non-uniform strain fields on the total strain energy density compared to uniform strain fields ($p = 0.648$). However, to help reduce the effect of friction and use the experimental procedure that includes global stresses and local strains, a thicker construct is recommended for mechanical stimulation, since the constructs that exhibited friction had an average thickness of 3.2 mm while the constructs without friction were 3.9 ± 0.2 mm.

There are a few notable limitations in this study. First, the local strains in the y-direction were assumed to be the same for the z-direction during the only tension loading condition. However, for the other loading conditions the strains in all directions were able to be measured because of the inclusion of compression, where strains in the z-direction were calculated based on the encoder values from the compressive actuator. Therefore, strains were able to be measured and recorded for all the loading conditions, except for

the only tension condition. Second, the thickness of the constructs influenced the strain pattern distribution in the x-direction, where constructs with an average thickness of 3.9 mm exhibited uniform strain fields indicating minimal friction. Thus, future studies should select thicker collagen constructs for mechanical stimulation. Third, the regression equation was developed using non-cellularized constructs and then used to convert from global to local strains in non-cellularized and cellularized constructs. Because the cellularized constructs showed an increase in tensile and compressive elastic moduli, the actual local strains may be greater than the predicted local strains from the regression equation. Thus, the regression equation used in this study to predict the local strains in cellularized constructs may actually underpredict the local strains. For future studies, a regression equation for cellularized constructs will be developed and included for the procedure of determining the predicted local elastic modulus for tension. Fourth, the effect of the sterilization procedure on the construct's structural integrity were not investigated. In future studies, a non-cellularized construct should be mechanical stimulated, sterilized, and then mechanical stimulated again to determine the influence of drying, ethanol, and UV light on the mechanical properties on the foam, such as the tensile and compressive elastic moduli. Fifth, water was used as the medium for mechanical stimulation. In future studies, cell media should be used as the medium to keep the cells alive during the mechanical stimulation, since water can cause the cells to lyse. Finally, only one magnitude of strain energy density was controlled and measured using the bioreactor. Therefore, the error between the targeted and actual strain energy density may increase or decrease depending on the user-selected strain energy density.

CHAPTER FOUR: CONCLUSIONS

4.1 Summary

In conclusion, this study found that a biaxial bioreactor can successfully control the total strain energy density in 3D cellular constructs while measuring the varying levels of distortion energy. These results will allow for the testing of new mechanobiology theories based on strain energy, which can potentially unify existing theories that only account for single directional loads (i.e. only tension, only compression). Furthermore, this novel method can help identify the mechanical mechanisms that trigger tissue remodeling, which would advance effective therapies for soft tissue pathology, such as manual therapy. The main contributions and findings of this work include:

- A validated methodology to apply differing levels of distortion to 3D cellularized constructs while maintaining a targeted strain energy density. To our knowledge, this is the first study to control total strain energy density in a localized region as well as measure distortion energy in 3D cellularized constructs.
- The finding that the type of loading condition had a significant effect on distortion and dilational energy, where the combined loading conditions experienced the greatest distortion and dilational energy compared to the simple loading conditions ($p < 0.0005$). Additionally, there was a significant difference between construct type on distortion and dilational

energy, where the cellularized constructs compared to the non-cellularized had the greatest distortion and dilational energy. Furthermore, the duration of stimulation cycles was found to have no significant effect on distortion or dilational energy.

- The finding that a low percent error could be achieved between the targeted and actual strain energy density using a novel bioreactor. This indicates that the converted local elastic modulus for tension was an accurate predictor to determine tensile forces that could reach the targeted strain energy density.

4.2 Challenges

During the completion of this research, there were several challenges that had to be addressed. One challenge was developing a repeatable method to apply uniform speckle patterns to all collagen constructs. Previous studies in the lab had used an airbrush with black, water insoluble ink to speckle soft tissue specimens, but this method was often inconsistent in applying uniform speckle patterns. Because the speckle pattern dictates the accuracy of the strain fields computed using DIC, it was important to develop a method that was repeatable. Various ‘DIC stamps’ were made from sandpaper and 3D printed parts, but these stamps could not produce crisp, clear speckle patterns. Thus, a commercially available DIC stamp was purchased, where uniform speckle patterns could consistently be applied to the collagen constructs with an average Shannon entropy of 4.8. Shannon entropy is used to analyze the contrast between the speckles and the background, where a number higher than 3 indicates a good contrast.

Another challenge was synching the stress data and strain data at the preferred cycles of 500, 1000, and 2000. The stress data was determined by the bioreactor force sensors while the strain data was calculated using the video recordings of construct deformation. In order to indicate the beginning of selected cycles during the video recording, a LED light had to be implemented into the LabVIEW program. The light was coded to turn on and off during the start and end of a selected cycle, respectively, and was placed within the view of the camera. Furthermore, the text file that output force and displacement data was revised to include cycle numbers. Therefore, the stress and strain data were then able to be synched at the selected cycles.

The last notable challenge was developing the Matlab code to calculate the distortion and dilational energy. Because strain energy density is equal to the area under the stress-strain curves, a Matlab code was created to determine the total strain energy density as well as the distortion and dilational components of the area under the curve. However, the stress-local strain curves were non-linear, thus the area had to be calculated using numerical integration techniques, such as approximating the area with rectangles and triangles. Additionally, the Matlab trapezoidal numerical integration function could not be used since the distortion and dilational components had to be calculated. In order to develop this code, the total strain energy density was first determined by calculating area as incremental triangles and rectangles and then comparing to the trapezoidal numerical integration function. Once completed, the distortion and dilational components were included, where cases of pure dilation and distortion were used to confirm the correct calculation of these components.

4.3 Future Work

In the near future, the biaxial bioreactor will be used determine the effect of dynamic distortion on cell behavior, matrix structure, and mechanical function in fibroblast-seeded constructs. The bioreactor will need to apply mechanical stimulation to 3D cellularized constructs during an *in vivo* culture period within an incubator. Therefore, the present experimental methodology used a regression equation to convert from global to local strains in order to predict the local tensile elastic modulus, which would allow for the prediction of tensile and compressive forces to achieve the targeted strain energy density with reasonable accuracy. An alternative approach would be to use DIC to periodically measure strain energy during in-vitro experiments, which would be time consuming and challenging due to the warm, humid environment of the incubator. The hypothesis of this future study will be the application of distortion energy to cellularized constructs will result in greater collagen expression and production, greater fiber alignment, and greater tensile elastic modulus. To achieve the hypothesis, fibroblast-seeded constructs will experience differing amounts of distortion energy during a 14-day culture period, which is a length of time commonly reported in literature for mechanical stimulation of tissue-like constructs [13,69,70]. The loading conditions for this study would consist of simple and complex loads. For the simple loads, only tension and only compression would be selected. For the complex loads, equal strain energy density in tension and compression would be selected, since this present study determined that this loading configuration resulted in the highest distortion energy. Because the other two complex loads did not show significant difference in strain energy density, future studies would select two new complex loading conditions with a larger difference in the strain

energy density shared between tension and compression. To analyze how tension and compression influence distortion energy, a larger difference would be necessary, where we would expect to see less distortion energy in these loading conditions compared to the equal strain density loading configuration.

Once mechanically stimulated, the mechanical properties of the constructs as well as the protein production and collagen alignment will be measured. The mechanical analysis will include the use of DIC techniques to determine the ultimate tensile strength, dynamic modulus, and stress relaxation. For the analysis of construct composition, methods will involve mass spectrometry for protein mass quantification and a laser-scanning confocal microscope to determine collagen organization with FiberFit software. These results will provide information on the specific mechanical mechanisms that stimulate fibroblasts to remodel and repair the collagen network, which could be used to better treat and prevent ligament and tendon injuries.

For future studies, cell viability in the constructs undergoing mechanical stimulation using the bioreactor in the incubator will be performed using an MTT assay. Once mechanical stimulation has been completed, the constructs will be removed in a biosafety cabinet to minimize bacterial contamination, where the constructs will be cut into several regions, such as the upper, middle, and lower gauge region. The upper and lower regions will have had experienced tension, while the middle region will have had been subjected to tension and compression. These pieces will then be placed into a 24-well plate, where the Dye and Solubilization Solution will be added according to the aforementioned protocol. Next, the absorbance of each region of the constructs will be measured using the plate reader, where cell viability will be determined for all regions

using the previously determined standard curve. By dividing the construct into different regions, the cell viability in each region will become apparent, where we would hypothesize that the middle region would have a higher cell viability compared to the other regions due to the addition of compression being applied.

REFERENCES

[1] L.H. Chen, M. Warner, L. Fingerhut, D. Makuc, Injury episodes and circumstances: National Health Interview Survey, Vital Heal. Stat. (2009).

[2] B.J. Erickson, G.L. Cvetanovich, B.U. Nwachukwu, L.D. Villarroel, J.L. Lin, B.R. Bach, F.M. McCormick, Trends in the management of achilles tendon ruptures in the united states medicare population, 2005-2011, Orthop. J. Sport Med. (2014).

[3] M.M. Herzog, S.W. Marshall, J.L. Lund, V. Pate, J.T. Spang, C. Hill, N. Carolina, Cost of Outpatient Arthroscopic Anterior Cruciate Ligament Reconstruction Among Commercially Insured Patients in the United, (2017) 1–8. doi:10.1177/2325967116684776.

[4] S.D. Joshi, K. Webb, Variation of cyclic strain parameters regulates development of elastic modulus in fibroblast/substrate constructs, J. Orthop. Res. 26 (2008) 1105–1113. doi:10.1002/jor.20626.

[5] C. Frank, S.L. Woo, D. Amiel, F. Harwood, M. Gomez, W. Akeson, Medial collateral ligament healing: A multidisciplinary assessment in rabbits., Am J Sport. Med. 11 (1983) 379–389.

[6] M.A. Gomez, S.L. Woo, M. Inoue, D. Amiel, F. Harwood, L. Kitabayashi, Medical collateral ligament healing subsequent to different treatment regimens., J Appl Physiol. 66 (1989) 245–252.

[7] R.M. van Rijn, A.G. van Os, R.M. Bernsen, P.A. Luijsterburg, B.W. Koes, S.M. Bierma-Zeinstra, What is the clinical course of acute ankle sprains? A systematic

literature review., Am J Med. 121 (2008) 324–331.

[8] J.D. Simpson, E.M. Stewart, D.M. Macias, H. Chander, A.C. Knight, Physical Therapy in Sport Individuals with chronic ankle instability exhibit dynamic postural stability de fi cits and altered unilateral landing biomechanics : A systematic review, Phys. Ther. Sport. 37 (2019) 210–219. doi:10.1016/j.ptsp.2018.06.003.

[9] N. Shrive, D. Chimich, L. Marchuk, J. Wilson, R. Brant, C. Frank, Soft-tissue "flaws" are associated with the material properties of the healing rabbit medial collateral ligament., J Orthop Res. 13 (1995) 923–929.

[10] R. Hauser, E. Dolan, Ligament Injury and Healing: An Overview of Current Clinical Concepts., J. Prolotherapy. (2011).

[11] D.P. Hart, L.E. Dahners, Healing of the medial collateral ligament in rats. The effects of repair, motion, and secondary stabilizing ligaments, J. Bone Jt. Surg. - Ser. 69 (1987) 1194–1199.

[12] J.A. Woo, M.A. Gomez, T.J. Sites, P.O. Newton, C.A. Orlando, W.H. Akeson, The biomechanical and morphological changes in the medial collateral ligament of the rabbit after immobilization and remobilization, J. Bone Jt. Surg. - Ser. 69 (1987) 1200–1211.

[13] H. Martínez, C. Brackmann, A. Enejder, P. Gatenholm, Mechanical stimulation of fibroblasts in micro-channeled bacterial cellulose scaffolds enhances production of oriented collagen fibers, J. Biomed. Mater. Res. - Part A. 100 A (2012) 948–957. doi:10.1002/jbm.a.34035.

[14] G. Yang, R.C. Crawford, J.H.C. Wang, Proliferation and collagen production of

human patellar tendon fibroblasts in response to cyclic uniaxial stretching in serum-free conditions, J. Biomech. 37 (2004) 1543–1550. doi:10.1016/j.jbiomech.2004.01.005.

[15] N. Juncosa-Melvin, K.S. Matlin, R.W. Holdcraft, V.S. Nirmalanandhan, D.L. Butler, Mechanical Stimulation Increases Collagen Type I and Collagen Type III Gene Expression of Stem Cell–Collagen Sponge Constructs for Patellar Tendon Repair, Tissue Eng. 13 (2007) 1219–1226. doi:10.1089/ten.2006.0339.

[16] K. Webb, R.W. Hitchcock, R.M. Smeal, W. Li, S.D. Gray, P.A. Tresco, Cyclic strain increases fibroblast proliferation, matrix accumulation, and elastic modulus of fibroblast-seeded polyurethane constructs, J. Biomech. 39 (2006) 1136–1144. doi:10.1016/j.jbiomech.2004.08.026.

[17] V.S. Nirmalanandhan, M.R. Dressler, J.T. Shearn, N. Juncosa-Melvin, M. Rao, C. Gooch, G. Bradica, D.L. Butler, Mechanical Stimulation of Tissue Engineered Tendon Constructs: Effect of Scaffold Materials, J. Biomech. Eng. 129 (2007) 919. doi:10.1115/1.2800828.

[18] C.B. Frank, Ligament structure , physiology and function, 4 (2004) 199–201.

[19] K.H. Wenger, A.R. El-Awady, R.L.W. Messer, M.M. Sharawy, G. White, C.A. Lapp, Pneumatic pressure bioreactor for cyclic hydrostatic stress application: mechanobiology effects on periodontal ligament cells, J. Appl. Physiol. 111 (2011) 1072–1079. doi:10.1152/japplphysiol.01175.2010.

[20] B. Boden, L. Griffin, W. Garrett, Etiology and Prevention of Noncontact ACL Injury., Phys Sport. 28 (2000) 53–60.

[21] N. Bates, R. Nesbitt, J. Shearn, G. Myer, T. Hewett, Relative strain in the anterior

cruciate ligament and medial collateral ligament during simulated jump landing and sidestep cutting tasks: implications for injury risk, Am J Sport. Med. 43 (2015) 2259–69.

[22] T. Best, A. Collins, E.G. Lilly, A. Seaber, Achilles tendon healing: A correlation between functional and mechanical performance in the rat, J. Orthop. Res. 11 (1993).

[23] R.A. Hauser, E.E. Dolan, H.J. Phillips, A.C. Newlin, R.E. Moore, B.A. Woldin, Ligament Injury and Healing : A Review of Current Clinical Diagnostics and Therapeutics, (2013) 1–20.

[24] M. Skutek, M. Van Griensven, J. Zeichen, N. Brauer, U. Bosch, Cyclic mechanical stretching modulates secretion pattern of growth factors in human tendon fibroblasts, Eur. J. Appl. Physiol. 86 (2001) 48–52. doi:10.1007/s004210100502.

[25] M. Skutek, M. Van Griensven, J. Zeichen, N. Brauer, U. Bosch, Cyclic mechanical stretching enhances secretion of Interleukin 6 in human tendon fibroblasts, Knee Surgery, Sport. Traumatol. Arthrosc. 9 (2001) 322–326. doi:10.1007/s001670100217.

[26] T. Molloy, Y. Wang, G. Murrell, The Roles of Growth Factors in Tendon and Ligament Healing, Sport. Med. 33 (2012).

[27] P.A. Torzilli, R. Grigiene, C. Huang, S.M. Friedman, S.B. Doty, A.L. Boskey, G. Lust, Characterization of cartilage metabolic response to static and dynamic stress using a mechanical explant test system, J. Biomech. 30 (1997) 1–9. doi:10.1016/S0021-9290(96)00117-0.

[28] J. Zeichen, M. van Griensven, U. Bosch, The proliferative response of isolated

human tendon fibroblasts to cyclic biaxial mechanical strain, Am J Sport. Med. 28 (2000) 888–892. http://www.ncbi.nlm.nih.gov/entrez/query.fcgi?cmd=Retrieve%7B&%7Ddb=PubMed%7B&%7Ddopt=Citation%7B&%7Dlist%7B_%7Duids=11101114.

[29] A. Papadopoulou, A. Iliadi, T. Eliades, D. Kletsas, Early responses of human periodontal ligament fibroblasts to cyclic and static mechanical stretching, Eur. J. Orthod. 39 (2017) 258–263. doi:10.1093/ejo/cjw075.

[30] S. Even-Ram, K.M. Yamada, Cell migration in 3D matrix, Curr. Opin. Cell Biol. 17 (2005) 524–532. doi:10.1016/j.ceb.2005.08.015.

[31] Z.H. Syedain, L.A. Meier, J.W. Bjork, A. Lee, R.T. Tranquillo, Implantable arterial grafts from human fibroblasts and fibrin using a multi-graft pulsed flow-stretch bioreactor with noninvasive strength monitoring, Biomaterials. 32 (2011) 714–722. doi:10.1016/j.biomaterials.2010.09.019.

[32] R.A. Lasher, J.C. Wolchok, M.K. Parikh, J.P. Kennedy, R.W. Hitchcock, Design and characterization of a modified T-flask bioreactor for continuous monitoring of engineered tissue stiffness, Biotechnol. Prog. 26 (2010) 857–864. doi:10.1002/btpr.380.

[33] Henshaw, Canine ACL Fibroblast Integrin Expression and Cell Alignment in Response to Cyclic Tensile Strain in Three-Dimensional Collagen Gels, Anticancer Res. 11 (1991) 1609–1612. doi:10.1002/jor.

[34] A. Petersen, P. Joly, C. Bergmann, G. Korus, G.N. Duda, The Impact of Substrate Stiffness and Mechanical Loading on Fibroblast-Induced Scaffold Remodeling, Tissue Eng. Part A. 18 (2012) 1804–1817. doi:10.1089/ten.tea.2011.0514.

[35] J.L. Balestrini, K.L. Billiar, Equibiaxial cyclic stretch stimulates fibroblasts to rapidly remodel fibrin, J. Biomech. 39 (2006) 2983–2990. doi:10.1016/j.jbiomech.2005.10.025.

[36] J.L. Balestrini, K.L. Billiar, Magnitude and duration of stretch modulate fibroblast remodeling., J. Biomech. Eng. 131 (2009) 051005. doi:10.1115/1.3049527.

[37] C. Biology, Taking Cell-Matrix Adhesions to the Third Dimension Edna Cukierman, Adv. Sci. 1708 (2008) 1708–1713.

[38] I. Martin, D. Wendt, M. Heberer, The role of bioreactors in tissue engineering, Trends Biotechnol. 22 (2004) 80–86. doi:10.1016/j.tibtech.2003.12.001.

[39] N. Plunkett, F.J. O'Brien, IV.3. Bioreactors in tissue engineering., Stud. Health Technol. Inform. 152 (2010) 214–230. doi:10.3233/THC-2011-0605.

[40] S.A. Korossis, F. Bolland, J.N. Kearnery, J. Fisher, E. Ingham, Bioreactors in Tissue Engineering, Top. Tissue Eng. 2 (2005).

[41] E. Oragui, M. Nannaparaju, W.S. Khan, The Role of Bioreactors in Tissue Engineering for Musculoskeletal Applications, Open Orthop. J. 5 (2011) 267–270.

[42] J.-J. Hu, J.D. Humphrey, A.T. Yeh, Characterization of Engineered Tissue Development Under Biaxial Stretch Using Nonlinear Optical Microscopy, Tissue Eng. Part A. 15 (2009) 1553–1564. doi:10.1089/ten.tea.2008.0287.

[43] Y. Bai, P.F. Lee, J.D. Humphrey, A.T. Yeh, Sequential multimodal microscopic imaging and biaxial mechanical testing of living multicomponent tissue constructs, Ann. Biomed. Eng. 42 (2014) 1791–1805. doi:10.1007/s10439-014-1019-3.

[44] K.A. Wartella, J.S. Wayne, Bioreactor for Biaxial Mechanical Stimulation to Tissue Engineered Constructs, J. Biomech. Eng. 131 (2009) 044501.

doi:10.1115/1.3049859.

[45] R. Budynas, J. Nisbett, Shigley's Mechanical Engineering Design, Tenth Edition, 2015.

[46] O.I. Okoli, The effects of strain rate and failure modes on the failure energy of fibre reinforced composites, Compos. Struct. 54 (2001) 299–303. doi:10.1016/S0263-8223(01)00101-5.

[47] Effect of expulsion on peak load and energy absorption of low carbon steel resistance spot welds, Sci. Technol. Weld. Join. 13 (2008) 39–43. doi:10.1179/174329307X249342.

[48] X. Sun, E. V. Stephens, M.A. Khaleel, Effects of fusion zone size and failure mode on peak load and energy absorption of advanced high strength steel spot welds under lap shear loading conditions, Eng. Fail. Anal. 15 (2008) 356–367. doi:10.1016/j.engfailanal.2007.01.018.

[49] F.R. Noyes, J.L. DeLucas, P.J. Torvik, Biomechanics of anterior cruciate ligament failure: an analysis of strain rate sensitivity and mechanisms of failure in primates, J. Bone Jt. Surg. - Ser. A. 56 (1974) 236–253. doi:10.2106/00004623-197456020-00002.

[50] G.K. Reddy, L. Stehno-Bittel, C.S. Enwemeka, Matrix remodeling in healing rabbit Achilles tendon, Wound Heal. Soc. (1999).

[51] S. Andrews, N. Shrive, J. Ronsky, The shocking truth about meniscus, J. Biomech. 44 (2011) 2737–2740. doi:10.1016/j.jbiomech.2011.08.026.

[52] J.G. Snedeker, M. Barbezat, P. Niederer, F.R. Schmidlin, M. Farshad, Strain energy density as a rupture criterion for the kidney: Impact tests on porcine organs,

finite element simulation, and a baseline comparison between human and porcine tissues, J. Biomech. (2005). doi:10.1016/j.jbiomech.2004.05.030.

[53] J.H. Keyak, S.A. Rossi, Prediction of femoral fracture load using finite element models: An examination of stress- and strain-based failure theories, J. Biomech. 33 (2000) 209–214. doi:10.1016/S0021-9290(99)00152-9.

[54] J.H. Keyak, S.A. Rossi, K.A. Jones, C.M. Les, H.B. Skinner, Prediction of fracture location in the proximal femur using finite element models, Med. Eng. Phys. 23 (2001) 657–664. doi:10.1016/S1350-4533(01)00094-7.

[55] C.A. Carmona-Moran, T.M. Wick, Transient Growth Factor Stimulation Improves Chondrogenesis in Static Culture and Under Dynamic Conditions in a Novel Shear and Perfusion Bioreactor, Cell. Mol. Bioeng. 8 (2015) 267–277. doi:10.1007/s12195-015-0387-6.

[56] A.H. Huang, B.M. Baker, G.A. Ateshian, R.L. Mauck, Sliding contact loading enhances the tensile properties of mesenchymal stem cell-seeded hydrogels, Eur. Cells Mater. 24 (2012) 29–45. doi:10.22203/eCM.v024a03.

[57] A. Hsieh, C. Tsai, Q. Ma, T. Lin, A. Banes, Time-dependent increases in type-III collagen gene expression in medical collateral ligament fibroblasts under cyclic strains., J. Orthop. Res. 18 (2005).

[58] T. Wang, P. Chen, M. Zheng, A. Wang, D. Lloyd, T. Leys, Q. Zheng, M.H. Zheng, In vitro loading models for tendon mechanobiology, J. Orthop. Res. 36 (2018) 566–575. doi:10.1002/jor.23752.

[59] G.H. Altman, H.H. Lu, R.L. Horan, T. Calabro, D. Ryder, D.L. Kaplan, P. Stark, I. Martin, J.C. Richmond, G. Vunjak-Novakovic, Advanced Bioreactor with

Controlled Application of Multi-Dimensional Strain For Tissue Engineering, J. Biomech. Eng. 124 (2002) 742. doi:10.1115/1.1519280.

[60] S.H. Mathes, L. Wohlwend, L. Uebersax, R. Von Mentlen, D.S. Thoma, R.E. Jung, C. GöRlach, U. Graf-Hausner, A bioreactor test system to mimic the biological and mechanical environment of oral soft tissues and to evaluate substitutes for connective tissue grafts, Biotechnol. Bioeng. 107 (2010) 1029–1039. doi:10.1002/bit.22893.

[61] Z. Luo, B. Seedhom, NCBINCBI Logo Skip to main content Skip to navigation Resources How To About NCBI Accesskeys PubMed US National Library of Medicine National Institutes of Health Search databaseSearch term Search AdvancedHelp Result Filters Format: AbstractSend to Proc In, Proc Inst Mech Eng H. 221 (2007).

[62] B.D. Elder, K.A. Athanasiou, Synergistic and additive effects of hydrostatic pressure and growth factors on tissue formation, PLoS One. 3 (2008). doi:10.1371/journal.pone.0002341.

[63] D. Kessler, S. Dethlefsen, I. Haase, M. Plomann, F. Hirche, T. Krieg, B. Eckes, Fibroblasts in Mechanically Stressed Collagen Lattices Assume a “Synthetic” Phenotype, J. Biol. Chem. 276 (2001) 36575–36585. doi:10.1074/jbc.M101602200.

[64] Z. Feng, Y. Tateishi, Y. Nomura, T. Kitajima, T. Nakamura, Construction of fibroblast-collagen gels with orientated fibrils induced by static or dynamic stress: Toward the fabrication of small tendon grafts, J. Artif. Organs. 9 (2006) 220–225. doi:10.1007/s10047-006-0354-z.

[65] L. Moradi, M. Vasei, M.M. Dehghan, M. Majidi, S. Farzad Mohajeri, S. Bonakdar, Regeneration of meniscus tissue using adipose mesenchymal stem cells-chondrocytes co-culture on a hybrid scaffold: In vivo study, Biomaterials. 126 (2017) 18–30. doi:10.1016/j.biomaterials.2017.02.022.

[66] R. Badaliance, Application of strain energy density factor to fatigue crack growth analysis, 13 (1980) 657–666.

[67] M. Neidert, E. Lee, T. Oegema, R. Tranquillo, Enhanced fibrin remodeling in vitro with TGF-beta1, insulin and plasmin for improved tissue-equivalents, Biomaterials. 17 (2002) 3717–31.

[68] M. Rubbens, A. Mol, T. Boerboom, R. Bank, F. Baaijens, C. Bouten, Intermittent straining accelerates the development of tissue properties in engineered heart valve tissue, Tissue Eng. Part A. 5 (2009) 999–1008.

[69] N. Juncosa-Melvin, G.P. Boivin, M.T. Galloway, C. Gooch, J.R. West, A.M. Sklenka, D.L. Butler, Effects of cell-to-collagen ratio in mesenchymal stem cell-seeded implants on tendon repair biomechanics and histology., Tissue Eng. 11 (2005) 448–57. doi:10.1089/ten.2005.11.448.

[70] N. Juncosa-melvin, D. Ph, J.T. Shearn, G.P. Boivin, C. Gooch, M.T. Galloway, J.R. West, S. Victor, G. Bradica, D.L. Butler, Effects of Mechanical Stimulation on Biomechanics and Histology of Stem Cell – Collagen Sponge Constructs for Rabbit Patellar Tendon Repair, Tissue Eng. 12 (2006).

[71] Ligament, (2019). https://en.wikipedia.org/wiki/Ligament.